Available online at www.sciencedirect.com
ScienceDirect
Journal of Pharmaceutical and Biomedical Analysis 43 (2007) 111–118
JOURNAL OF PHARMACEUTICAL AND BIOMEDICAL ANALYSIS
www.elsevier.com/locate/jpba

Acid–base equilibrium of puerarin in CTAB micelles

Juqun Xi, Rong Guo *

School of Chemistry and Chemical Engineering, Yangzhou University, Yangzhou 225002, People's Republic of China

Received 5 April 2006; received in revised form 4 June 2006; accepted 8 June 2006
Available online 28 August 2006

Abstract

Electronic absorption spectra, fluorescence emission spectra, ^{1}HNMR and ab initio quantum calculation are used to study the acid–base equilibrium of puerarin in cetytrimethylammonium bromide (CTAB) micelles with different microstructures and microenvironments. Experiments suggest the microenvironment provided by CTAB micelle cause the acid–base equilibrium of puerarin to move to the deprotonation reaction. The changes in the chemical shifts of the individual groups of protons in CTAB indicate that the location of puerarin changes from the inner to the outer of the CTAB micelles with an increase in puerarin concentration, which enhances the interaction between puerarin and CTAB. The binding of puerarin with CTAB micelle is a spontaneous ($\Delta G < 0$) and endothermic process ($\Delta H < 0$), and the hydrophobic and electrostatic force is the main driving force for its solubilization.

Keywords: Puerarin; CTAB; Micelles; Acid–base equilibrium; Binding constant; Partition coefficient

1. Introduction

Flavonoids are natural compounds that are effective scavengers of active oxygen radicals such as hydroxyl and superoxide radicals. Moreover, recent investigations indicate that some of them show antitumor, antibacterial, and antiinflammatory activities [1–4]. Puerarin, a naturally occurring isoflavone C-glycoside, is isolated from pueraria lobota [5], one of the most popular Chinese herbal medicines that is traditionally used to reduce febrile symptoms and is also used as an antiinebriation agent [6]. The chemical name of this compound is 8-β-D-glucopyransyl-7-hydroxy-3-(4-hydroxyphenyl)-4H-1-benzopyran-4-one. Fig. 1 shows the chemical structure of puerarin. The biomedical effects of puerarin, which have been experimentally or clinically demonstrated [7,8], include the improvement of blood circulation, prevention of cardiovascular diseases, control of alcoholism, and treatment for arrhythmia [9,10].

As we know, drug interactions with heterogeneous media (micelles, vesicles, biomembranes) induce changes in some physicochemical properties of drugs (solubility, spectroscopic and acid–base properties) [11,12]. Moreover, puerarin's polyphenolic structure makes it very sensitive to the change in its structure and the polarity of the environment. Quantification of the effect of micelles in acid–base and solubilization properties of pharmaceutical drugs can be used for the determination of binding constants drug/micelle. These constants can be determined if there is at least one molecular property that changes when the drug is transferred from water to the micellar medium. As this variation is related with changes in the microenvironment of the molecule undergoing solubilization, it can provide a detailed picture for partitioning of the neutral form of the drug in the micellar pseudophase, and a picture of the interactions of the charged form with micelle surface. In the present paper, the acid–base equilibrium of puerarin in CTAB micelles was studied by electronic absorption spectra, fluorescence emission spectra, ^{1}HNMR and molecular modeling study. The binding constant and distribution coefficient were determined.

2. Materials and methods

2.1. Chemicals

Puerarin of pharmaceutical purity grade was kindly provided Nanjing Chemical Reagent Plant (China). All samples of puerarin were dried in vacuum at (105–110 °C) for 2 h, and used without further purification. Cetytrimethylammonium bromide (CTAB) was purchased from Sigma–Aldrich

* Corresponding author. Tel.: +86 514 7975219; fax: +86 514 7311374.
E-mail address: guorong@yzu.edu.cn (R. Guo).

0731-7085/$ – see front matter © 2006 Published by Elsevier B.V.
doi:10.1016/j.jpba.2006.06.028

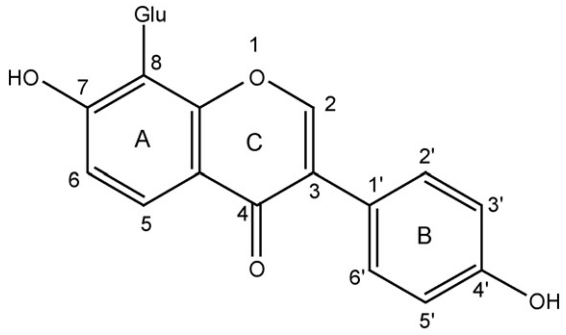

Fig. 1. Structure of puerarin.

Chemical Co. (St. Louis, MO). The water used was double distilled.

2.2. UV–vis spectra measurements

Puerarin was dissolved in the CTAB micelles, and after 1 h of mixing, the spectra were recorded by using a UV-2550 spectrophotometer (Shimadzu) in the wavelength range of 200–450 nm. Distilled water was used as blank.

2.3. Measurement of the pK values for puerarin

pH was measured with pH acidity meter (Leizi Instrumental Factory, Shanghai). The pH of the solution was adjusted by using aliquots of concentrated solutions of NaOH and HCl. Values of pK were determined spectrophotometrically according to Henderson–Hasselbatch equation [13]:

$$pK = pH - \ln \frac{\alpha}{100 - \alpha} \quad (1)$$

where α is the percentage of groups that have been ionized. Values for α are obtained from the absorbance at 345 nm for pK_1 and 260 nm for pK_2 of puerarin. The 0% ionization value and the 100% ionization value can be calculated from the values of absorbance at both ends of puerarin titration curves, as in extremely acid media (pH $\ll$ pK) all puearin exists in uncharged form, while in extremely alkaline media (pH $\gg$ pK) the predominant species exist in charged form.

2.4. Ab initio quantum calculation

Geometries were fully optimized at the HF/6-311G level using the Gaussian 03 program. Force constant analyses were performed to verify the minimum energy state of the optimized geometries as well as to obtain zero-point energies (ZPE) and thermal corrections to the energy. Energy evaluations were carried out at the MP2/6-311G level on the HF/6-311G(d) optimized geometries [14].

2.5. The study of ^{1}HNMR spectra

The ^{1}HNMR spectra were recorded on a Bruker AV-600 at 600 MHz (^{1}H) spectrometer using the pulsed FTNMR technique.

2.6. Fluorescence spectral measurements

The fluorescence spectra of puerarin were recorded with an RF-5301 PC spectrofluorophotometer (Shimadzu) in the wavelength range of 380–600 nm with the excitation wavelength being 330 nm. Its fluorescence polarization P was measured by inserting polarization filters on the excitation and emission light paths of fluorescence spectrophotometer. The emission intensities of the polarized light, parallel and vertical to the excitation-polarized light, $I_{||}$ and $I_{\perp}$, were combined together to calculate the steady-state polarization P:

$$P = \frac{I_{||} - I_{\perp}}{I_{||} + I_{\perp}} \quad (2)$$

3. Results and discussion

Flavonoids consist of a benzene ring fused with a γ-pyrone ring, which are usually denoted by A- and C-rings, respectively. The most important chemical property of flavonoids is the enhanced reactivity of the C-ring whereas the A-ring usually reacts as an aromatic ring. More specifically, the acid–base properties of the C-ring have been subject of a number of studies since protonation of substrates occurs during numerous biochemical processes and, in some cases, it is the key step of the entire process [15,16]. The puerarin molecule has two deprotonation sites (pK_1, pK_2) at the oxygen atoms at position 4′ and 7 (Fig. 1). Energy evaluations show that the bond energy of hydroxyl group at position 4′ (−50.8 kcal/mol) on ring-B is lower than that at position 7 (−53.6 kcal/mol) on ring-A. According to these results, we can state that the hydroxyl group at position 4′ is a stronger acid than that at position 7, which makes reliable predictions of the acid–base properties [17,18]. So, puerarin undergoes acid dissociation reactions like the following (see Scheme 1 for details).

UV spectra of flavonoids exhibit two major absorption bands in the region 200–400 nm. Band-I (300–380 nm) is considered to be associated with absorption due to the ring-B cinnamoyl system and band-II (200–280 nm) is considered to be associated with absorption due to the ring-A benzoyl system [19]. Fig. 2 shows the UV absorption spectra of aqueous solution of

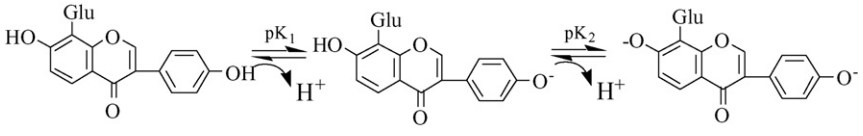

Scheme 1. Acid–base equilibrium reactions of puerarin.

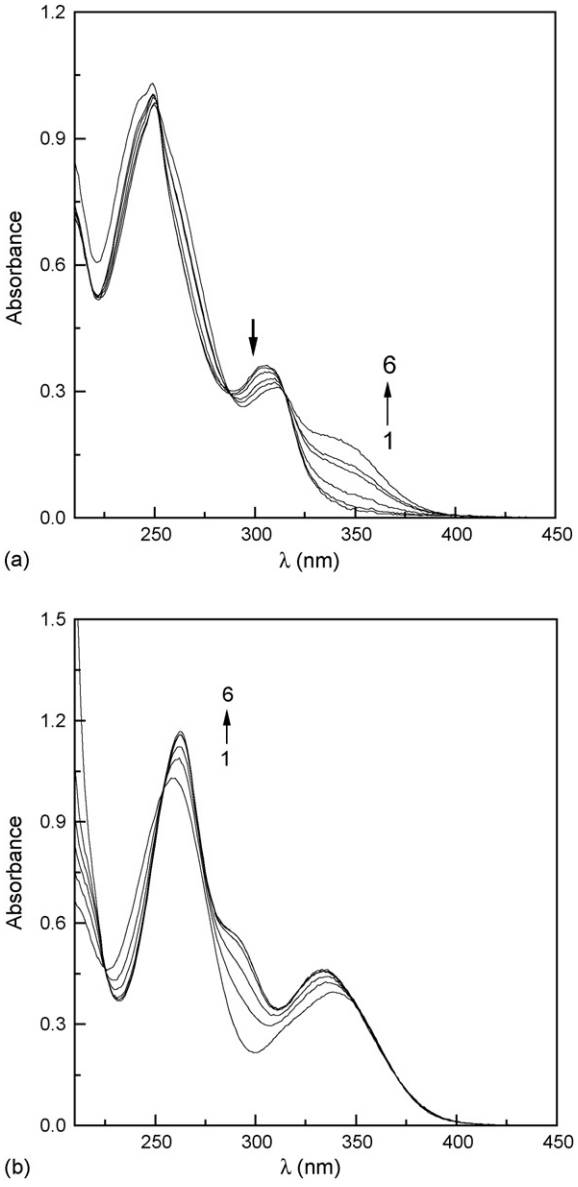

Fig. 2. Absorption spectra of puerarin ($c = 3.0 \times 10^{-5}$ mol L^{-1}) in different pH conditions of aqueous solutions. (a) pH values: (1) 2.99, (2) 5.24, (3) 6.35, (4) 7.22, (5) 7.98, (6) 8.90. (b) pH values: (1) 9.97, (2) 10.34, (3) 10.70, (4) 11.10, (5) 11.49, (6) 12.26.

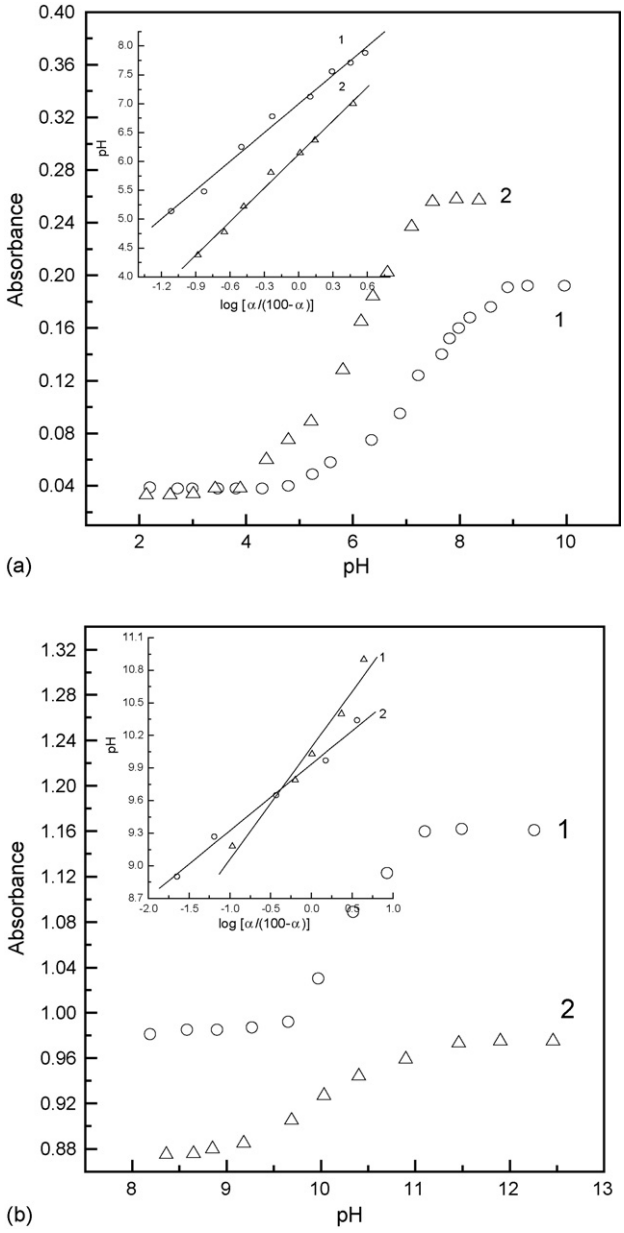

Fig. 3. Plots of absorbance at (a) 345 nm and (b) 260 nm as a function of pH. (Inset) Plots of ratio between molecular and charged species as function of pH. (1) Aqueous solution; (2) CTAB micelles ($c = 8.0 \times 10^{-3}$ mol L^{-1}).

puerarin at different pH values. The uncharged form (H_2Pu) of puerarin has an absorption maximum at 306 nm, which decreases upon increasing pH values, giving rise to the monoanionic form (HPu^-) with a maximum at 345 nm (Fig. 2(a)). For the second equilibrium (Fig. 2(b)), around a pH close to pK_2 the peak at 260 nm due to the dianionic forms of puerarin increases and shows a red shift [20]. In the studied range of pH values, it is evident that tow isosbestic points exist at the wavelength point where the spectra cross up (315 nm (Fig. 2(a) and 254 nm (Fig. 2(b)). In the case of puerarin, tow isosbestic points can be identified as conforming to the presence of three chemical species participating in two acid–base equilibria: (a) uncharged (H_2Pu) and monoanionic (HPu^-) forms, (b) monoanionic (HPu^-) and dianionic forms (Pu^{2-}) within pH ranges around the pK_1 and pK_2, respectively. Fig. 3 shows the experimental values of observed absorbance vs. pH values. A plot of the pH of the solution as a function of log $[\alpha/(100-\alpha)]$ yielded a straight line with an intercept on the pH axis (at log $[\alpha/(100-\alpha)] = 0$) equal to p$K$ (inset, Fig. 3). The pK_1 and pK_2 obtained (pK^w) are 6.91 and 9.93. When CTAB micelles are present in the medium, the values of pK^m obtained are 6.12 and 9.78.

The pK shift, ΔpK (=pK^w − pK^m), is a consequence of the different partition coefficients for the charged and uncharged species. ΔpK can be positive, zero, or negative, depending on solute and membrane surface charge [21]. We measured the partition coefficients (P_{WM}) for H_2Pu and Pu^{2-} between micelles and aqueous phase at pH 2.1 (pH ≪ pK_1) and (pH ≫ pK_2),

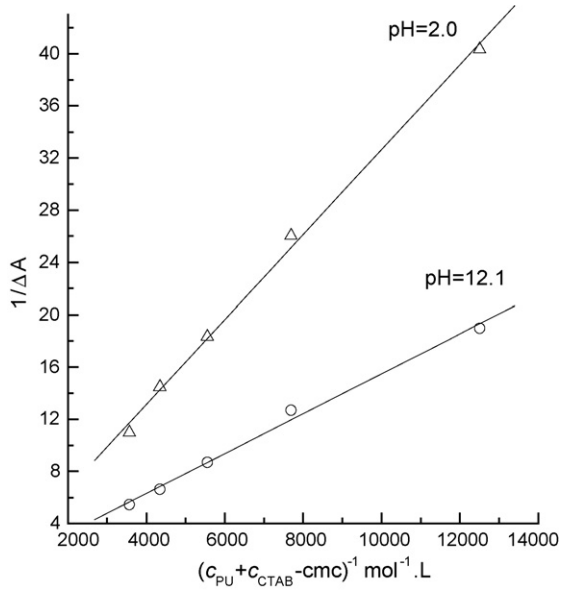

Fig. 4. Relation between $1/\Delta A$ and $1/(c_{pu} + c_{CTAB} - cmc)$ for puerarin ($c = 3.0 \times 10^{-5}$ mol L^{-1}) in CTAB micelles (cmc $\approx 2.0 \times 10^{-4}$ mol L^{-1}, determined by method of surface tension).

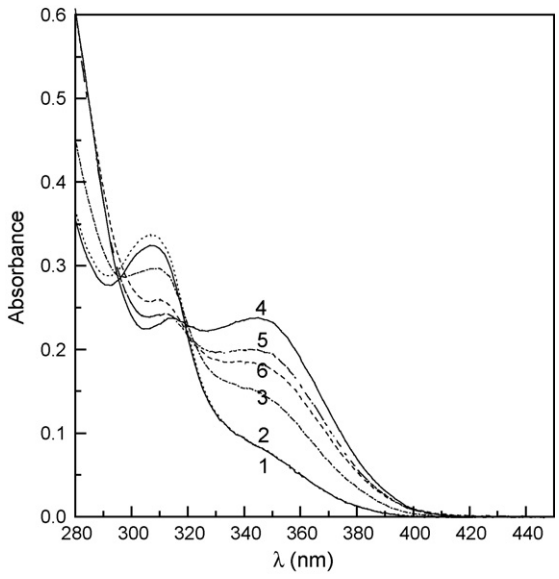

Fig. 5. Absorption spectra of puerarin ($c = 3.0 \times 10^{-5}$ mol L^{-1}) in different CTAB micelles. CTAB (mol L^{-1}): (1) 0.0, (2) 1.0×10^{-4}, (3) 9.2×10^{-4}, (4) 8.0×10^{-3}, (5) 3.0×10^{-2}, (6) 5.0×10^{-2}.

respectively. The method used for calculating partition coefficients was described in a recent paper (see Eqs. (12)–(16) of ref. [22]). The results show that Pu^{2-} exhibits larger partition coefficient (6992.6) than that of H_2Pu (2056.2) (Fig. 4). The partition coefficients for charged and uncharged forms are different and the negatively charged form of puerarin shows the greater affinity to positively charged CTAB micelle surface, which lead the lowering of pK in micellar solutions ($\Delta pK_1 = 0.53$, $\Delta pK_2 = 0.15$). On the other hand, the concentration of H^+ is decreased on CTAB micelle surface due to the electrostatic repulsion force between H^+ and CTA^+, which also cause the acid–base equilibrium of puerarin to move to the deprotonation reaction. Both of these factors cause the lowering of pK value in micellar solutions.

As we know, with increasing CTAB content, CTAB can form pre-micellar aggregates before the first critical micelle concentration (cmc1), spherical micelle after cmc1, and rod-like micelle after cmc2 in the aqueous solution. The cmc1 and cmc2 are found to be 8.6×10^{-4} mol L^{-1} and 2.0×10^{-2} mol L^{-1} with addition of puerarin (5.0×10^{-5} mol L^{-1}) by the methods of conductivity, and the report values of cmc for CTAB are 8.9×10^{-4} mol L^{-1} and 2.2×10^{-2} mol L^{-1}. Fig. 5 represents the absorption spectra of puerarin in the CTAB micelles with different structures at pH value of 7.02. In this condition, a mixture of uncharged and monoanionic forms of puerarin exists. The CTAB pre-micellar aggregates exert nearly no influence on the puerarin absorption spectra (curve 2 in Fig. 5). The CTAB spherical micelle causes a red shift for band I from 306 to 314 nm. The isosbestic point of puerarin absorption also appears in CTAB spherical micelles, which is very similar to the increasing pH value (curves 3 and 4 in Fig. 5). However, the CTAB rod-like micelles cause the opposite trend in the absorption spectra (curves 5 and 6 in Fig. 5). As a result, the acid–base equilibrium of puerarin is inevitably influenced by the different structures and microenvironments of the CTAB micelles.

Micelles can be pictured as having a non-polar interior and a relatively polar interfacial region. The interior of the micelle is generally considered to be the locus of solubilization for non-polar solubilizate such as *n*-alkanes [23]. Puerarin has aromatic rings and its solubility in water is not high and it exists in the anionic state with one charge, while CTAB is a kind of cationic surfactant. Puerarin will be easily extracted into the micelle. Here, the microenvironment provided by CTAB micelles promote the deproton of puerarin and enhance their interaction [24]. This result has been confirmed by the lowering of pK in micellar solutions ($\Delta pK_1 = 0.53$, $\Delta pK_2 = 0.15$).

The different effects of spherical and rod-like CTAB micelle on puerarin can also be seen from Fig. 6. When the CTAB con-

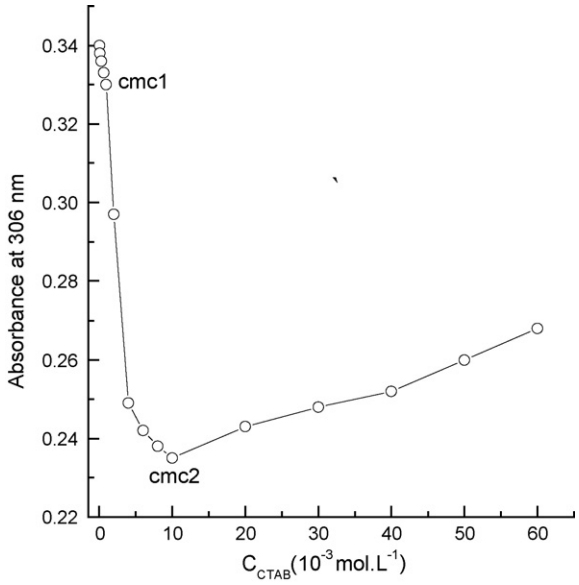

Fig. 6. Influence of CTAB concentration on the absorbance of puerarin ($c = 3.0 \times 10^{-5}$ mol L^{-1}).

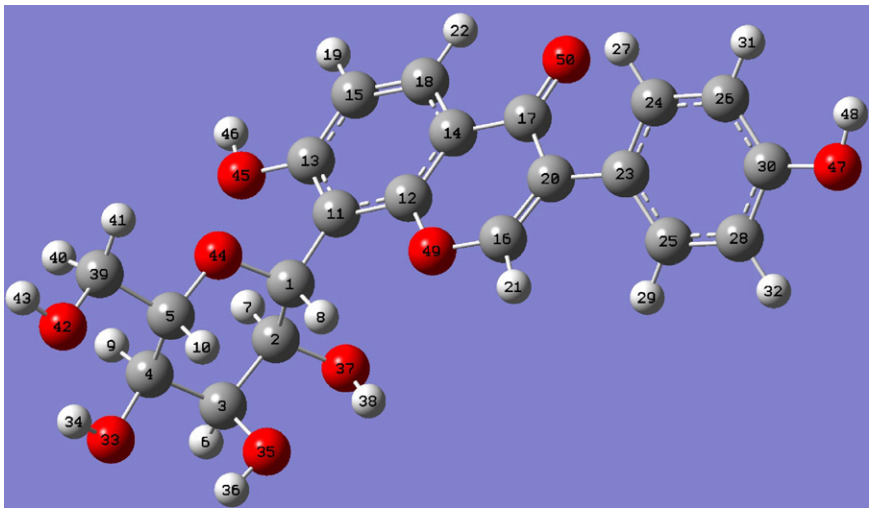

Fig. 7. Optimized structure of puerarin molecule.

centration is lower than cmc1, the uncharged form of puerarin (H_2Pu) gives a maximum at 306 nm, which exhibits almost no change with CTAB concentration; when the CTAB concentration arrives at cmc1, the absorbance at 306 nm decreases, giving rise to the absorbance of (HPu^-) at 345 nm; when the CTAB concentration is higher than cmc2, the absorbance at 306 nm increases suddenly. The two inflections on the curve (Fig. 6) correspond well to the structural change of CTAB micelle from spherical to rod-like. By comparison, the structure of the spherical micelle is not so compact and it can provide a relatively large solubilization space for puerarin, so puerarin mainly exists in CTAB micelle. When puerarin is added to the CTAB rod-like micelle, the decreasing solubilization space and the more compact structure no longer permit more puerarin molecules to be located in CTAB micelle, and, as a result, puerarin is mainly located in aqueous phase, which leads the movement of acid–base equilibrium to the left side. That is to say spherical micelles will favor the displacement of the equilibrium towards the base, while rod-like micelles will favor the displacement towards the acid form.

Which part of puerarin can be located and where the puerarin is solubilized in the CTAB micelles are both of great importance to the understanding of the interaction between puerarin and CTAB micelles and of acid–base equilibrium of puerarin. The optimisation of the puerarin molecule by ab initio quantum chemical calculations show that the stable structure of puerarin is not planar, but with the B-ring connected to the C-ring by a single C–C bond around which rotation can occur, the B-ring deviates with 38.59° from the planarity (Fig. 7). We deduce that puerarin is very likely to interact with the CTAB micelles with the B-ring part of the molecule (Fig. 1). A reliable and convenient method to assess the solubilization site of a solubilizate in an aqueous micellar system is provided by ^{1}HNMR spectroscopy. The ^{1}HNMR spectrum of micellized CTAB is characterized by resonance signals corresponding to six groups of protons, which are designated in the following [25]:

e c-d b a a'
CH_3—$(CH_2)_{13}$—CH_2—CH_2—$N^+(CH_3)_3Br^-$

The chemical shifts (δ) of individual groups of the protons in CTAB with and without puerarin are listed in Table 1. The concentration of CTAB and the pH value are kept constant at 8.0×10^{-3} mol L^{-1} and 7.02, respectively. In this condition, uncharged and monoanionic forms of puerarin co-exist. The changes in <delta> of protons caused by addition of puerarin could be well explained based on the shielding effect of aromatic rings of puerarin [26,27]. It can be seen from Table 1 that the increase of m ($m = C_{puerarin}/C_{CTAB} \times 100$) almost has no obvious influence on the chemical shift of d-H and e-H. This indicates that the aromatic rings of puerarin are far away from the terminal e-H, which is located in the very core of the micelle. When m is lower than 10, the increaseing puerarin concentration has weak effect on the chemical shift of a′-H and a-H, but obvious influence on the chemical shift of b-H and c-H. This shows that puerarin exists a little far from the polar side of –N(CH3)$_3$, while it is near the long chain of the inner alkyl of the micelles. When m is higher than 10, the line of a′-H and a-H obviously moved to the up field with the increase of puerarin concentration. This indicates that the location of puerarin makes a change from the inner to the outer of the CTAB micelles, which made a′-H and a-H locate above or under the plane of the aromatic ring of puerarin. So we can deduce that puerarin will move to

Table 1
Chemical shifts (ppm) of individual groups of protons in the presence of puerarin

e c-d b a a'
CH_3—$(CH_2)_{13}$—CH_2—CH_2—$N^+(CH_3)_3Br^-$

$m = 100C_{puerarin}/C_{CTAB}$	CTAB					
	a-H	a′-H	b-H	c-H	d-H	e-H
0	3.313	3.088	1.691	1.299	1.209	0.796
5	3.312	3.086	1.688	1.293	1.209	0.796
10	3.310	3.085	1.684	1.296	1.208	0.795
20	3.304	3.079	1.684	1.288	1.206	0.794
40	3.302	3.073	1.683	1.284	1.206	0.795
$\Delta\delta$	0.011	0.015	0.008	0.015	0.003	0.001

Concentration of CTAB is 8.0×10^{-3} mol L^{-1}.

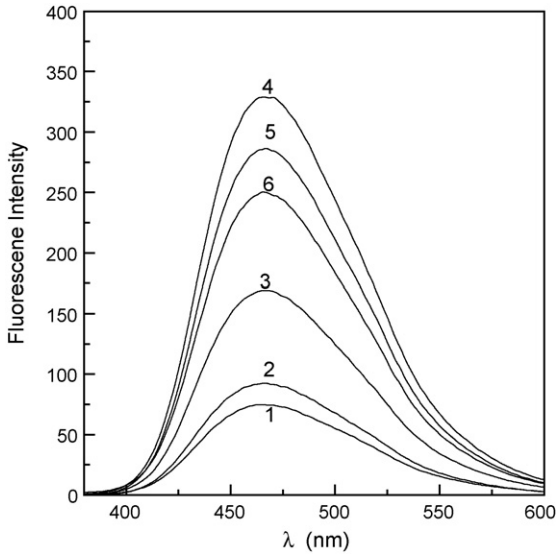

Fig. 8. Influence of CTAB concentration on the fluorescence intensity of puerarin ($c = 3.0 \times 10^{-5}$ mol L^{-1}). CTAB (mol L^{-1}): (1) 0.0, (2) 1.0×10^{-4}, (3) 9.2×10^{-4}, (4) 8.0×10^{-3}, (5) 3.0×10^{-2}, (6) 5.0×10^{-2}. The excited wavelength is 330 nm and the emission wavelength is 470 nm.

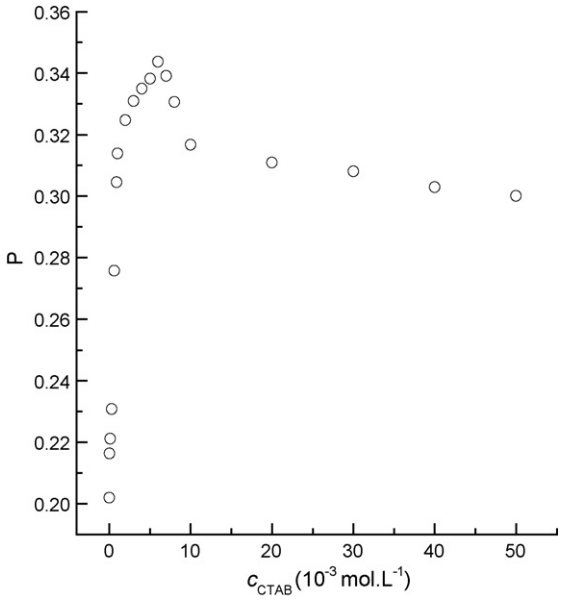

Fig. 9. Variation in the fluorescence polarization (P) of puerarin ($c = 3.0 \times 10^{-5}$ mol L^{-1}) with CTAB concentration. The excited wavelength is 330 nm and the emission wavelength is 470 nm.

the edge of the micelles. Because of the location on the edge of micelles, the electrostatic force between negatively charged puerarin and the polar groups of CTAB micelles is increased, which will promote the deprotonation reaction of puerarin and cause a rightward shift of equilibrium. Such dynamic process of puerarin's location in CTAB micelles induces the change in its acid–base properties to the deprotonation reaction.

The interaction of puerarin with CTAB micelles is further studied by the fluorescence method. Fluorescence spectra of puerarin at pH 7.02 are depicted in Fig. 8. In this condition, both uncharged (H_2Pu) and monoanionic (HPu^-) forms co-exist and the fluorescence spectra for both species exhibited peaks at around 470 nm with the excitation wavelength being 330 nm. So the fluorescence polarization (P), binding constant (K) and partition coefficient (P_{MW}) are affected by both uncharged and monoanionic forms of puerarin.

When puerarin is mixed with CTAB micelles, its fluorescence intensity is increased markedly (curves 1–4 in Fig. 8). When the CTAB concentration is higher than cmc2, the fluorescence intensity of puerarin decreases suddenly (curves 5 and 6 Fig. 8). This result is due to the different solubilized space provided by spherical and rod-like micelles. With the B-ring of the puerarin molecule solubilized in the CTAB micelle, the rotation of the B-ring is limited, the planarity of the whole molecule is increased and the π conjugation is extended, eventually leading to the increase of its fluorescence intensity. When puerarin is added to the CTAB rod-like micelle, the decreasing solubilization space and the more compact structure no longer permit more puerarin molecules to be located in CTAB micelle, and as a result, puerarin is mainly located in aqueous phase, so the fluorescence intensity is reduced.

The plot of the fluorescence polarization (P) against the CTAB concentration will further prove the above interpretation. As we know, the fluorescence polarization (P) has a relationship with the molecular rotation velocity and the microviscosity [28]. The changes in the fluorescence polarization (P) of puerarin with the CTAB concentration are shown in Fig. 9. It can be seen that, when the concentration of CTAB is below cmc2, the values of the P increase continuously with increasing CTAB concentration, which means the molecular rotation velocity of puerarin is decreased as a result of its solubilization into the micelle which cause a lowering of pK in micellar solutions. But when the CTAB micelle changes to rod-like (above cmc2), the fluorescence polarization (P) shows a little decrease. The decreasing solubilization space and more compact structure of the rod-like micelle accounts for this, with the room for the puerarin decreasing, the number of puerarin molecules being tied is decreased and the number of free puerarin molecules is increased. So, more and more puerarin molecules exist in aqueous phase in uncharged form, which also results in a rightward shift of acid–base equilibrium. As a result, the molecular rotation velocity of puerarin is increased and the value of P decreases. This result is accordant with the above conclusions about those of the UV–vis and fluorescence spectra.

The model employed to determine the binding constant between fluorescent molecules and spherical micelles is based on the fluorescence quantum yields in both aqueous and ordered micelles. The binding constant, K, is obtained from the following equation [29]:

$$\left[\left(\frac{I}{I_0}\right) - 1\right]^{-1} = \left[\left(\frac{I_M}{I_0}\right) - 1\right]^{-1} \left[1 + \frac{1}{(\gamma K C_S)}\right] \quad (3)$$

Here, I is the fluorescence intensity of the system, I_0 the fluorescence intensity of the system in the absence of micelle, I_M the maximum fluorescence intensity obtained, C_S the concentration of the surfactant, and γ the quenching coefficient ($\gamma = 1$). However, because the increase of puerarin fluorescence intensity

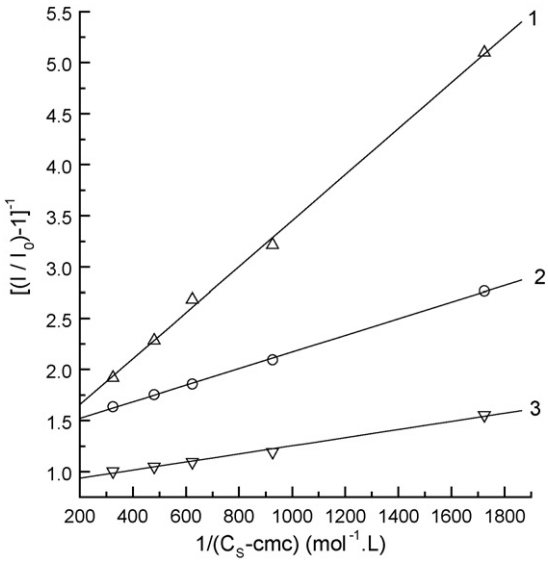

Fig. 10. Plotting of $[(I/I_0)-1]^{-1}$ vs. $1/(C_S - \text{cmc})$. Concentration of puerarin (mol L^{-1}): (1) 1.0×10^{-5}, (2) 3.0×10^{-5}, (3) 5.0×10^{-5}.

always takes place at concentrations higher than the first critical micelle concentration, the corresponding C_S values must be changed to a micellar form, C_M, expressed by:

$$C_M = C_S - \text{cmc} \tag{4}$$

Therefore, by substitution of Eq. (4) into Eq. (3), an expression which relates the increase of fluorescence intensity with the concentration of micellized surfactant can be obtained:

$$\left[\left(\frac{I}{I_0}\right) - 1\right]^{-1} = \left[\left(\frac{I_M}{I_0}\right) - 1\right]^{-1} \left[+\frac{1}{\gamma K(C_S - \text{cmc})}\right] \tag{5}$$

The plot of $[(I/I_0)-1]^{-1}$ versus $1/(C_S - \text{cmc})$ gives a straight line, and the value of the binding constant can be obtained from the quotient of the intercept and slope of this line (Fig. 10). The distribution coefficient (P_{MW}) of puerarin between the CTAB micellar phase and the bulk aqueous phase can be obtained through the following equation [30]:

$$K = (P_{MW} - 1)\bar{V} \tag{6}$$

where K is the binding constant, P_{MW} the distribution coefficient, and $\overline{V}$ the partial molar volume ($\overline{V}_{CTAB}$ is 0.37 L/mol [31]). Table 2 shows the binding constant K and the distribution coefficient P_{MW} of puerarin in CTAB micelles, respectively. As Table 2 shows, the higher the puearin concentration is, the larger the values of the partiotion coefficient and binding constant of

Table 2
Binding constant K and partition coefficient P_{MW} in different concentrations of puerarin in CTAB micelles

T (°C)	Puerarin (10^{-5} mol L^{-1})	K	P_{MW}
25.0	1.0	543.9	1484.8
	3.0	1672.1	4520.2
	5.0	2148.3	5807.2

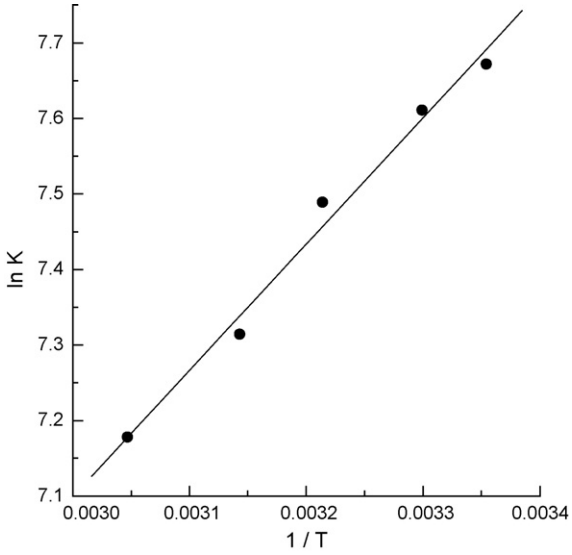

Fig. 11. Linear dependence of the ln K on $1/T$.

puerarin. The binding constant is related to standard Gibbs free energy ΔG° by the equation of $\Delta G^\circ = -RT \ln K$. The increase in concentration of puerarin affects the aggregation number of CTAB micelles and causes the change of the ΔG° value, so the binding constant and partition coefficient are changed along with the concentration of puerarin. The larger values of K and P_{MW} mean more and more puerarin molecules are located in CTAB micelles, and the electrostatic force between the negatively charged puerarin and cationic CTAB (CTA^+) is enhanced, which will be favor the movement of acid–base equilibrium to the right side.

The thermodynamics functions of the binding process can be calculated from the following equations:

$$\Delta G = -RT \ln K \tag{7}$$

$$\ln K = -\frac{\Delta H}{R}\left(\frac{1}{T}\right) + C \tag{8}$$

Table 3
Binding constant of puerarin with CTAB micelles and the thermodynamic functions of the binding process

T (°C)	Puerarin (10^{-5} mol L^{-1})	K	ΔG (kJ mol^{-1})	ΔS (J mol^{-1} K^{-1})	ΔH (kJ mol^{-1})
25.0		2148.3	−19.02	17.15	
30.0		2021.2	−19.17	17.38	
38.0	5.0	1788.3	−19.37	17.57	−13.90
45.0		1500.7	−19.34	17.10	
55.0		1310.2	−19.58	17.30	

$$\Delta G = \Delta H - T\Delta S \quad (9)$$

Here ΔG is the Gibbs free energy, ΔH the enthalpy, C a constant, and T the absolute temperature. The slope of the plot of $\ln K$ vs. $1/T$ can be used to calculate the enthalpy (ΔH) (Fig. 11). Table 3 shows the binding constant K and the thermodynamics functions of the binding process. From Table 3, we can see that the binding of puerarin to the CTAB micelles is a spontaneous behavior ($\Delta G < 0$), $\Delta H < 0$ indicating the process of puerarin interaction with the CTAB micelles is an exothermic process. The rise in the temperature is unfavorable to the location of the puerarin in the CTAB micelles. Thus, the value of K decreases with increasing temperature accordingly. In addition, the value of ΔH (−17.03 kJ/mol) is smaller than that of the interaction energy of the chemical bond (>100 kJ/mol) [32], indicating the interaction force between puerarin and CTAB micelle is a weak intermolecular force (mainly the electrostatic and hydrophobic force).

4. Conclusions

Puerarin, isolated from Pueraria lobota, is one of the most popular Chinese herbal medicines that is traditionally used to reduce febrile symptoms and is also used as an antiinebriation agent. In this paper, the acid–base properties of puerarin in CTAB micelles are studied by electronic absorption, fluorescence emission, ^{1}HNMR measurements, and the ab initio quantum calculation. Experiments suggest that with the increasing puerarin concentration, the NMR chemical shifts of a-H and a′-H in CTAB obviously decrease, this indicates the solubilization location of puerarin in CTAB moves from inner to the outer of CTAB micelles. This dynamic process of puerarin's localization in CTAB micelles causes the acid–base equilibrium of puerarinto move to the deprotonation reaction, enhancing the interaction between puerarin and CTAB, and promoting the formation of the puerarin–CTAB associate. The interaction between puerarin and micelles (binding constant and distribution coefficient) also affects the acid–base properties of puerarin.

Acknowledgment

This work is supported by the National Natural Scientific Foundation of China (20233010).

References

[1] P. Gamache, E. Ryan, I.N. Acworth, J. Chromatogr. 635 (1993) 143–150.
[2] L. Coward, N. Barnes, K. Setchell, S. Barnes, J. Agric. Food Chem. 41 (1993) 1961–1967.
[3] S.W. Lamson, M.S. Brignall, Alt. Med. Rev. 5 (2000) 196–208.
[4] Pharmacopoeia of the People's Republic of China, vol. 1, Chemical Industry Press, Beijing, 2000, pp. 273.
[5] Z. Guo, Q. Jin, G. Fan, Y. Duan, C. Qin, M. Wen, Anal. Chim. Acta 436 (2001) 41–47.
[6] D.H. Overstreet, W.M. Keung, A.H. Rezvani, M. Massi, D.Y.W. Lee, Alcohol.: Clin. Exp. Res. 27 (2003) 177–185.
[7] J.H. Zhu, X.X. Wang, J.Z. Chen, Acta Pharmacol. Sin. 25 (2004) 1045–1051.
[8] R. Cervellati, C. Renzulli, M.C. Guerra, E. Speroni, J. Agric. Food Chem. 50 (2002) 7504–7750.
[9] E. Benlhabib, J.I. Baker, D.E. Keyler, A.K. Singh, J. Med. Food 7 (2004) 180–186.
[10] L. Ding, Y. Yang, S. Han, Puerarin injection for perfusion for treating heart disease. CN1249178.
[11] P.M. Saikia, M. Bora, R.K. Dutta, J. Coll. Interf. Sci. 285 (2005) 382–387.
[12] H. Chakraborty, M. Sarkar, Biophys. Chem. 117 (2005) 79–85.
[13] R. Sabaté, M. Gallardo, J. Estelrich, J. Coll. Interf. Sci. 233 (2001) 205–210.
[14] C. Alemán, J. Mol. Struct.—Theochem. 528 (2000) 65–73.
[15] K. Venkataraman, Methods for determining the structure of flavonoids compounds, in: T.A. Geissman (Ed.), The Chemistry of Flavonoids Compounds, MacMillan, New York, 1962.
[16] D.A. García, M.A. Perillo, Biochim. Biophy. Acta 1418 (1999) 221–231.
[17] D.J. Defrees, A.D. Mclean, J. Comput. Chem. 7 (1986) 321–333.
[18] C. Colomines, M. Orozco, F.J. Luque, J.I. Borrell, J.A. Teixido, J. Org. Chem. 63 (1998) 4947–4953.
[19] F. Zsila, Z. Bikadi, M. Simonyi, Biochem. Pharmacol. 65 (2003) 447–456.
[20] M.D. Engelmann, R. Hutcheson, I.F. Cheng, J. Agric. Food Chem. 53 (2005) 2950–2953.
[21] S. Schreier, S.V.P. Malheiros, E.D. Paula, Biochim. Biophys. Acta 1508 (2000) 210–234.
[22] O. Čudina, K.K. Rajić, I.R. Bugarčić, I. Janković, Coll. Surf. A 256 (2005) 225–232.
[23] J.H. Fendler, L.K. Patterson, J. Phys. Chem. 75 (1971) 3907.
[24] Y.H. Zhang, Y.Q. Liang, J. Chin. Univ. 15 (1994) 266–269.
[25] H.Z. Yuan, S. Zhao, G.Z. Cheng, L. Zhang, X.J. Miao, S.Z. Mao, J.Y. Yu, L.F. Shen, Y.R. Du, J. Phys. Chem. 105 (2001) 4611–4615.
[26] M. Graetzel, K. Kalyanasundaram, J.K. Thomas, J. Am. Chem. Soc. 96 (1974) 7869–7874.
[27] X. Huang, W. Zhang, Z. Zhang, G. Xu, C. Li, Spectrochim. Acta Part A 54 (1998) 617–621.
[28] W.Y. Liu, R. Guo, J. Coll. Interf. Sci. 290 (2005) 564–573.
[29] M.D.L. Guardia, E.P. Cardells, J. Sancenon, J.L. Carrion, E. Pramauro, Microchem. J. 44 (1991) 193–200.
[30] G.P. Song, R. Guo, Y.F. Yang, J. Yangzhou Technol. Coll. (Nat. Sci.) 12 (1992) 42–47.
[31] I.M. Cuccovia, E.H. Schroeter, P.M. Monteiro, H. Chaimovich, J. Org. Chem. 43 (1978) 2248–2252.
[32] R. Guo, W.Y. Liu, G.K. Fan, Acta Phys.-Chim. Sin. 17 (2001) 1062–1066.